

RESEARCH

Open Access



Charaterizations of 3D printed re-entrant pattern/aramid knit composite prepared by various tilting angles

Imjoo Jung¹, Hyelim Kim² and Sunhee Lee^{3*} 

*Correspondence:
shlee014@dau.ac.kr

³ Professor, Department
of Fashion Design,
Dong-A University, 37
Nakdong-Daero, Saha-gu,
Busan 49315, Republic
of Korea
Full list of author information
is available at the end of the
article

Abstract

This study intended to compare and analyze the Poisson's ratio and mechanical properties of aramid knit (ARNT), 3D printed auxetic re-entrant pattern (3DP-RE), and 2 types of composite fabrics manufactured with ARNT and 3DP-RE. Specimens were manufactured by 3D printing the re-entrant pattern with a CFDM (conveyor fused deposition modeling) 3D printer and TPU (thermoplastic polyurethane) filament, combining with aramid knit in 2 ways. Then, Poisson's ratio, bending, compression, and tensile properties were tested. As a result of Poisson's ratio, 3DP-RE and its 2 types of composite fabric showed negative Poisson's ratio at all angles and deformed stable at 0° and 90° than the bias direction. The bending strength confirmed that the composite fabric showed a lower value. But, the strain at max bending strength was greater than a substrate fabric. At the compression properties, it has been confirmed that compression strength and toughness are improved when manufacturing composite fabrics. As a result of tensile properties, 3DP-RE and composite fabrics were significantly more initial modulus, elongation and toughness than ARNT and were shown to be the largest in gradient 90°. Therefore, it is confirmed that the performance is excellent when fabricated as a 3DP-RE/ARNT composite fabric, and based on the results of studies, we intend to use it as the basic data for composite fabrics of auxetic structure suitable for shoe uppers.

Keywords: Aramid knit, Auxetic re-entrant pattern, 3D Printed Composite Fabric, Thermoplastic polyurethane (TPU), Mechanical property

Introduction

The aramid has better performance in high strength, high elasticity, high heat resistance, dimensional stability, and insulating properties than other fibers. It's applied to safety equipments such as foot wear, gloves and socks in the fields of defense and fire-fighting, in various forms such as yarn, fabric, nonwoven fabric, and knit. Such aramid is broadly divided into m-Aramid and p-Aramid. The m-Aramid is mainly used for combat uniforms, military tents, air suits, etc. that require heat resistance, anti-inflammatory, friction resistance, etc., while the p-Aramid is mainly used for bulletproof clothing, firefighting uniforms, safety shoes, safety helmets, etc. that require high strength, high elasticity, cutting resistance, etc. (Han & Lee, 2006; Han et al., 2011). Accordingly,

the development of safety shoes and safety clothing products using this aramid is also steadily progressing (Abtew et al., 2019; Jung et al., 2019; Shoes Upper Fabric Development, 2020). Furthermore, to improve the properties of such aramid-based materials, researches are underway to improve shock absorption as a protective material by manufacturing them in composite fabrics along with rubber and polyurethane-based materials (Roy et al., 2018; Wang et al., 2020).

The re-entrant structure is a typical auxetic structure having a negative Poisson's ratio and has a bow-tie shape. The auxetic re-entrant structure represents higher yield strengths and energy absorptions than other structures (Kolken & Zadpoor, 2017; Lakes, 2017). Recently, researches are underway to manufacture it as fabrics such as polyurethane and knit with high elasticity by using the excellent characteristics of auxetic structures, or to manufacture it as a composite fabric by laminating with other fabrics to improve the performance of fabrics (Kamrul et al., 2020; Li & Wang, 2017; Novak et al., 2020; Zhao et al., 2020).

A composite fabric generally refers to a fabric with improved performance different from the conventional one by polymerizing two or more components of different characteristics. One of the methods for manufacturing a composite fabric is the laminate, which can improve the strength and durability by laminating layers of each fabric. Thereby, the combination of fabric and auxetic material provides excellent durability such as shape stability, negative Poisson's ratio, and energy absorption. Novak et al. (2020) attempted to compare tensile properties and the Poisson's ratios by laser-cutting the cellulose-based weft knitted fabric and the EVA (ethylene–vinyl–acetate) foam material in re-entrant and chiral structures and manufacturing specimens laminated with a rubber-based adhesive (Neostik). They confirmed that the strength was increased during tensile test and the Poisson's ratio was decreased than the untreated fabric after laminating it as a composite fabric. In addition, they also confirmed that shape stability was given by the reduction in width strain in the machine direction compared to the untreated fabric, and they reported that the strain of the re-entrant structure was less and more stable at low strain.

Recently, there has been an increasing tendency for researches combining the excellent properties of auxetic materials with 3D printing technology, and researches on performance improvement by laminating it with fabrics have also been conducted (Grimmelsmann et al., 2016; Li et al., 2018; Yang et al., 2018). Grimmelsmann et al. (2016) printed various types of threads, knit structures, and 3D printed auxetic structures on them by number and angle of printing layers, and they measured and compared the morphology, the ellipticity of the pore of the knitted fabric and the tensile properties through tensile test. By 3D printing the auxetic structure to the knit, it was confirmed that the shape was stable and tensile strength was improved during the tensile test. The papers reported so have been found to have analyzed the mechanical properties, mainly by directly printing with a 3D printer on the fabric. Our research team is conducting research to manufacture textiles using FDM 3D printing technology and auxetic structures. As a previous study, Lee (2018) conducted basic research on how to manufacture 3D printed textiles by directly printing laces on the voile fabric with FDM 3D printing technology to manufacture composite materials and measuring mechanical properties and washability. Recently,

based on this, Kim and Lee (2020) evaluated the auxetic properties by measuring the mechanical properties of re-entrant patterns by TPU hardness. Kabir et al. (2020a) manufactured a composite fabric by printing directly on the nylon fabric with a FDM 3D printer, and analyzed its characteristics. After that, Kabir et al. (2020b) confirmed the shape memory properties and physical properties through the heating process to confirm its applicability to the shoe uppers by printing the sinusoidal patterns directly on the nylon fabric with a shape memory thermoplastic polyurethane filament. In addition, Kim et al. (2020) manufactured a composite fabric by laminating the 3D printed auxetic re-entrant pattern and neoprene, and confirmed the mechanical properties to determine its applicability to aqua shoes and surf boots for wetsuit.

Therefore, in this study, we attempted to compare and analyze the aramid knit, the 3D printed auxetic re-entrant pattern, and two composite fabrics laminating the two in consideration of the Poisson's ratio at five different tilting angles and mechanical properties. The specimens were manufactured by laminating with a one meter long re-entrant pattern printed by a CFDM (conveyor fused deposition modeling) 3D printer in two directions for each aramid knit, and cut by five tilting angles of 0°, 30°, 45°, 60° and 90°. The properties of auxetic have been identified through tests on Poisson's ratio, bending properties, compression properties and tensile properties. Based on the results of the research, we intend to use it as a basis for composite fabrics of auxetic structure suitable for shoe uppers.

Methods

Materials

A conveyor-type FDM (CFDM, conveyor fused deposition modeling) process 3D printer (Blackbelt, Netherland) and a 0.6 mm diameter nozzle were used to print a 3D printed auxetic re-entrant pattern. The filament used is a thermoplastic polyurethane-based (TPU) filament (Ninjaflex, NinjaTek, USA) suitable for clothing products, and has a diameter of 1.75 mm and a hardness of 85 A. For the manufacture of 3D printed auxetic re-entrant pattern/textile composite fabrics, the aramid knit, a raw fabric with a thickness of 1 mm and a weight of 0.018 g/cm² (Mirae advanced material Co. Ltd., Korea) was used, and for the laminate, spray adhesive (3 M 77, 3 M, USA) was used.

Preparations of 3D printed auxetic re-entrant pattern/aramid knit composite with various tilting angles

The 3D printed auxetic re-entrant pattern was manufactured in the same way as the previous study (Kim et al., 2020). In addition, as shown in Fig. 1, using a 3D printed auxetic re-entrant pattern (3DP-RE), a 3D printed auxetic re-entrant/aramid knit composite fabric (3DP-RE/ARNT) was manufactured in two ways by aramid knit fabric direction. First, the aramid knit (ARNT) was placed in MD (machine direction). And the 3DP-RE was rotated at five tilting angles of 0°, 30°, 45°, 60°, and 90°; and then was bonded to be cut to the size of each experimental condition. Next, the ARNT and 3DP-RE was positioned and bonded in the MD; was rotated at five tilting angles of 0°, 30°, 45°, 60°, and 90°; and then was prepared by cutting them according to the experimental condition.

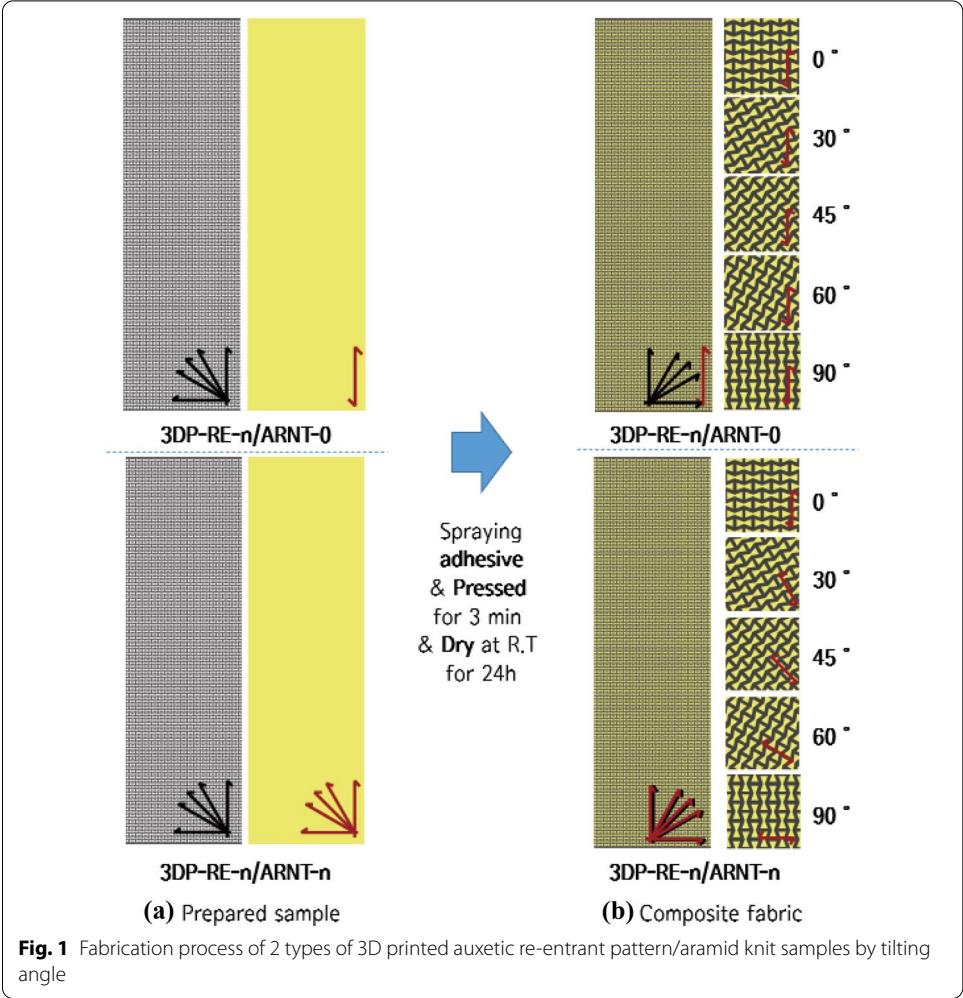

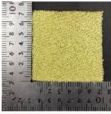
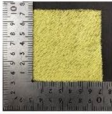



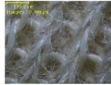
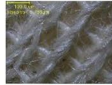
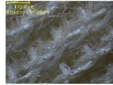
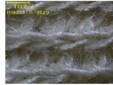
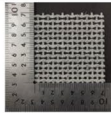
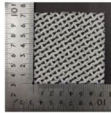
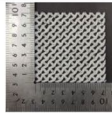

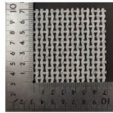
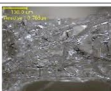

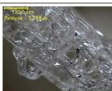
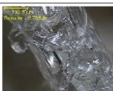
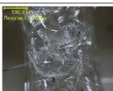
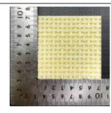
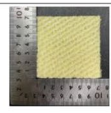
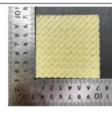
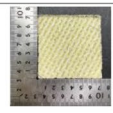
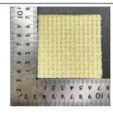

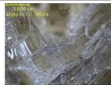
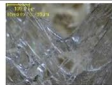
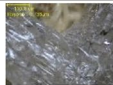
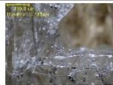
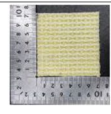
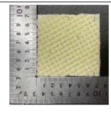
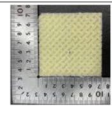
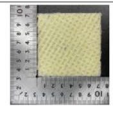
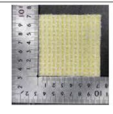
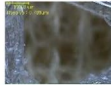






Table 1 Sample code of aramid knit, 3D printing auxetic re-entrant pattern and 2 types of 3D printed auxetic re-entrant pattern/aramid knit samples by tilting angle

Angle (°)	Aramid knit-*n	3D printing auxetic re-entrant pattern-*n	3D printing auxetic re-entrant pattern-*n/ Aramid knit-0	3D printing auxetic re-entrant pattern-*n/ Aramid knit-*n
0	ARNT-0	3DP-RE-0	3DP-RE-0/ARNT-0	3DP-RE-0/ARNT-0
30	ARNT-30	3DP-RE-30	3DP-RE-30/ARNT-0	3DP-RE-30/ARNT-30
45	ARNT-45	3DP-RE-45	3DP-RE-45/ARNT-0	3DP-RE-45/ARNT-45
60	ARNT-60	3DP-RE-60	3DP-RE-60/ARNT-0	3DP-RE-60/ARNT-60
90	ARNT-90	3DP-RE-90	3DP-RE-90/ARNT-0	3DP-RE-90/ARNT-90

The bonding method for the manufacture of 3DP-RE and ARNT composite fabric is to evenly apply 3 M strong adhesive spray to the back of the 3DP-RE; bond it to the ARNT; then press and dry at room temperature for 24 h before use. Each sample code and sample image are listed in Tables 1 and 2.

Table 2 Sample images of aramid knit, 3D printed auxetic re-entrant pattern and 2 types of 3D printed auxetic re-entrant pattern/aramid knit samples by tilting angle

Type		Tilt angle (°)				
Sample	Image	0	30	45	60	90
ARNT-n	Digital					
	Surface					
	*t (mm)	1.0				
3DP-RE-n	Digital					
	Surface					
	*t (mm)	2.0				
3DP-RE-n/ ARNT-0	Digital					
	Surface					
	*t (mm)	3.0				
3DP-RE-n/ ARNT-n	Digital					
	Surface					
	*t (mm)	3.0				

Characterizations

Poisson's ratio

Poisson's ratio was measured to confirm the auxetic properties of the 3D printed auxetic re-entrant pattern and two types of 3D printed auxetic re-entrant/aramid knit composite fabric. The Poisson's ratio was conducted according to the KS M ISO 527 (Korean Standard Association [KSA], 2017a) standard. Uniaxial tensile was performed with a universal testing machine (AGS-X, SHIMADZU, Japan), and the average value was used after the Poisson's ratio of two units was measured by Eq. (1). ν is the Poisson's ratio, E_t

and ϵ_l is the average value of the transverse strain and longitudinal strain. The measurement positions are shown in Table 3. The specimen size was determined to be 25 mm in width \times 75 mm in length respectively, and the size was measured under conditions of a gauge length of 25 mm and a tensile speed of 25 mm/min. During the tensile experiment, the experimental video was taken with a digital camera (HDR-CX550, Sony Corp., Japan) for 0 to 20 s, and the Poisson's ratio was calculated by the following equation with a strain of 0% to 30% via the image obtained from the video.

$$\nu = -\frac{\epsilon_t}{\epsilon_l} \quad (1)$$

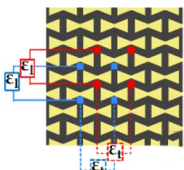
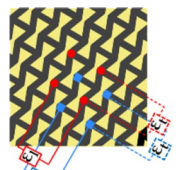
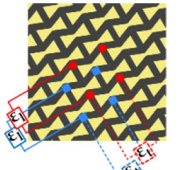
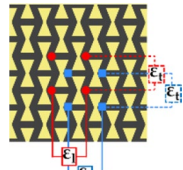
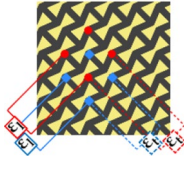
Note. ϵ_t : average of transverse strain; ϵ_l : average of longitudinal or axial strain.

Bending test

To confirm the bending properties the test was conducted according to the experimental method of the previous study (Kim et al., 2020). The bending test was conducted according to the KS M ISO 14125 (Korean Standard Association [KSA], 2017b) standard using a universal testing machine (AGS-X, Shimadzu, Japan). The specimen size was 75 mm in width \times 25 mm in length, and was prepared with five tilting angles of 0°, 30°, 45°, 60°, and 90°. The speed was set to 2 mm/min and the distance between the lower points was set to 62.5 mm. A bending strength-strain curve was obtained by testing, and the bending strength of each material was calculated using Eq. (2) below. The value of each result was used as an average value after being measured three times.

$$\sigma_f = \frac{3PL}{2bd^2} \quad (2)$$

Table 3 Measurement position of Poisson's ratio for 3D printed auxetic re-entrant pattern and 2 types of 3D printed auxetic re-entrant pattern/aramid knit by tilting angle

Angle(°)	Measurement position	Angle(°)	Measurement position
0		60	
30		90	
45			

where, P : load at a given point on the load deflection curve(N); L : support span(mm); b : width of test beam(mm); d : depth or thickness of tested beam(mm).

Compression test

To confirm the compressive properties by tilting angles of the 3D printed re-entrant pattern, the compressive properties were measured according to the experimental method of the previous study (Kim et al., 2020). Experiments were conducted using a 5kN load cell in the universal testing machine (AGS-X, Semaz, Japan). The specimen were prepared in a size of 75 mm in width \times 25 mm in length, and were compressed in the -z direction and at a speed of 10 mm/min according to the KS M ISO 602 standard. The maximum load was limited to 4.75 kN in order not to destroy the specimen. Each sample was compressed three times and the obtained average value was used to analyze the strength at 50% strain and toughness.

Tensile test

To confirm the tensile properties of the composite fabric by tilting angles of the 3D printed re-entrant pattern, the measurement was conducted according to the KS M ISO 14125 standard using a universal testing machine (AGS-X, SHIMADZU, Japan). Each sample was prepared in a size of 25 mm in width \times 75 mm in length, and the experiment was conducted under the conditions of a distance between clamps of 25 mm and a tensile speed of 50 mm/min. The initial elasticity and toughness are confirmed using the stress–strain curve obtained by the tensile experiments. To compare and analyze the tensile properties of aramid knit, 3D printed auxetic re-entrant pattern and 2 types of composite fabrics, each breaking strength, elongation at breaking strength, max strength, and elongation at max strength were confirmed. In the experiment, the average value obtained after measuring 3 times for each sample was used.

Results and Discussion

Poisson's ratio of 3D printed auxetic re-entrant pattern and its two-types of composite fabrics by tilting angles

Poisson's ratio is the ratio of lateral strain and axial strain that shrinks or expands when a load is applied in the tensile direction of the material, and the auxetic structure has a negative Poisson's ratio (Kolken & Zadpoor, 2017; Lakes, 2017). In this study, to apply the re-entrant structure to the shoe uppers according to the previous study (Kim et al., 2020), we measured the Poisson's ratio by two tilting angles of the 3D printed auxetic re-entrant pattern and the 3D printed auxetic re-entrant pattern/aramid knit composite fabric to confirm that they are auxetic structures. The Poisson's ratio values for each tilting angle when tensioned to increase the strain from 0 to 30% are shown in Fig. 2.

The 3DP-RE-n in Fig. 2a showed negative values at all tilting angles and was identified as an auxetic structure. The Poisson's ratio by tilting angles was measured as $-0.18 \sim 0.00$, $-0.65 \sim -0.09$, $-0.47 \sim -0.14$, $-1.06 \sim -0.28$, and $-0.17 \sim 0.00$; were in the order of $3DP-RE-90 > 3DP-RE-0 > 3DP-RE-30 > 3DP-RE-45 > 3DP-RE-60$. 3DP-RE-0 and 3DP-RE-90 values were close to 0 because the units of the re-entrant structure were oriented parallel or vertically in the tensile direction, resulting in greater strain in the tensile direction. In addition, 3DP-RE-60 is considered to have appeared a lot of shear

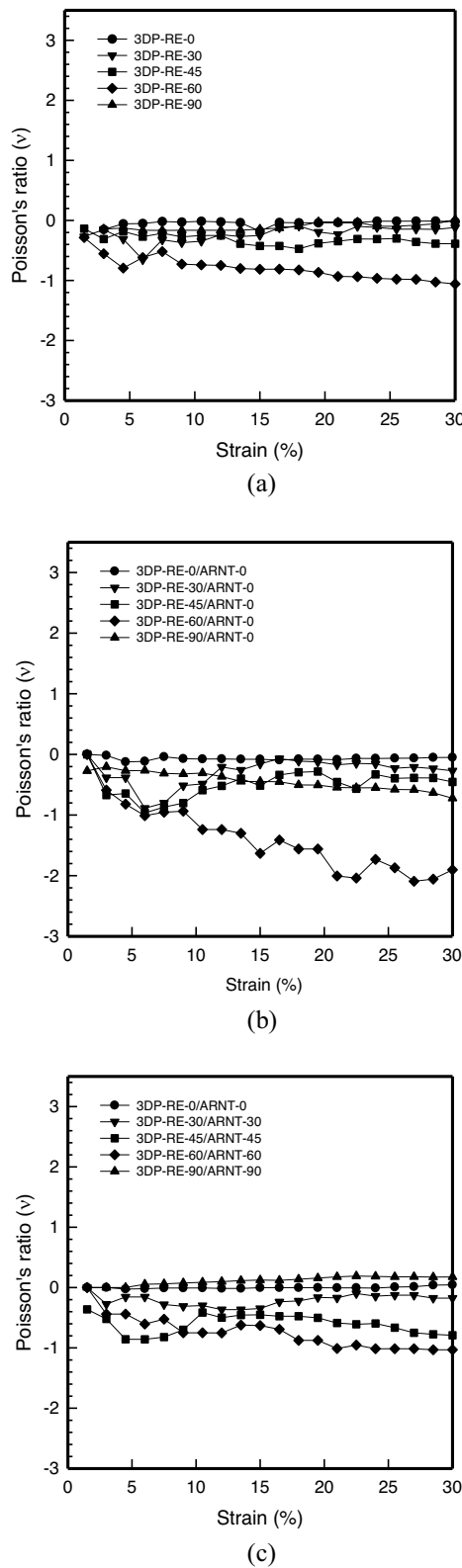


Fig. 2 Poisson's ratio of 3D printed auxetic re-entrant pattern and 2 types of 3D printed auxetic re-entrant pattern/aramid knit composite with various tilting angles

deformation because the units of the re-entrant structure were most inclined in the tensile direction.

3DP-RE-n/ARNT-0 in Fig. 2b also showed a negative values at all tilting angles. The Poisson's ratio by tilting angles is measured as $-0.12-0.00$, $-0.89-0.00$, $-0.96-0.00$, $-2.09-0.00$; appeared larger in the order of 3DP-RE-0/ARNT-0 > 3DP-RE-90/ARNT-0 > 3DP-RE-30/ARNT-0 > 3DP-RE-45/ARNT-0 > 3DP-RE-60/ARNT-0. Similar to the 3DP-RE-n, it was measured closer to 0 at 0° and 90° rather than the bias directions of 30° , 45° and 60° , and the strain of 3DP-RE-60/ARNT-0 was the greatest under the influence of the 3D printed auxetic re-entrant pattern.

The Poisson's ratio by tilting angles of 3DP-RE-n/ARNT-n in Fig. 2c was measured as $-0.03-0.05$, $-0.37-0.00$, $-0.86-0.36$, $-1.03-0.00$, and $0.00-0.19$; appeared larger in the order of 3DP-RE-90/ARNT-90 > 3DP-RE-0/ARNT-0 > 3DP-RE-30/ARNT-30 > 3DP-RE-45/ARNT-45 > 3DP-RE-60/ARNT-60. The 3DP-RE-30/ARNT-30, 3DP-RE-45/ARNT-45, and 3DP-RE-60/ARNT-60 in the bias direction were all identified as having negative Poisson's ratios, and were confirmed to be auxetic structures, however, 3DP-RE-0/ARNT-0 showed a positive Poisson's ratio from a strain of 25.5%.

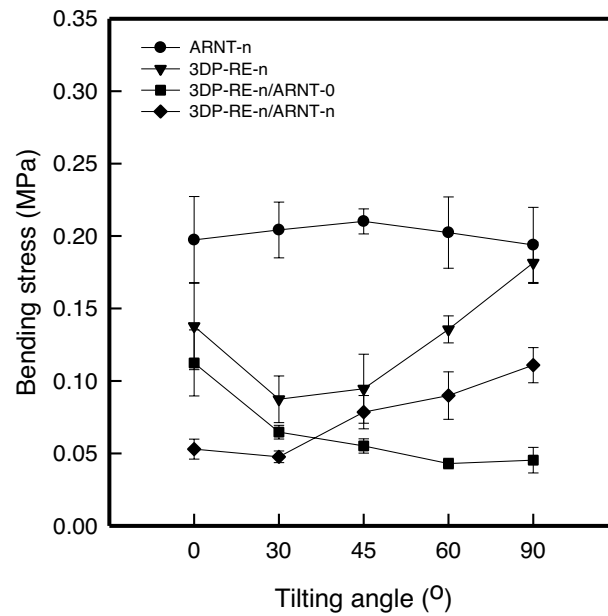
In addition, the Poisson's ratio of 3DP-RE-n/ARNT-n is more stable than that of 3DP-RE-n/ARNT-0. It is considered to have been easier to tensile because the tilting angle of the 3D printed auxetic re-entrant pattern and aramid fabric were applied equally, and the 3D printed re-entrant pattern had a greater effect than the aramid fabric.

Bending property of aramid knit, 3D printed auxetic re-entrant pattern and its two-types of composite fabrics by tilting angles

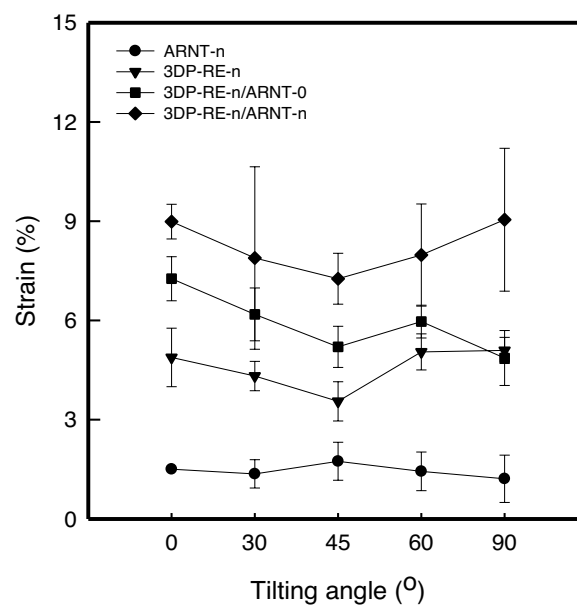
The bending test has recently been used to analyze mechanical properties when 3D printed materials are given a constant load (Li & Wang et al., 2017). This present study investigated the bending properties by pattern tilting angle of the aramid knit, the 3D printed auxetic re-entrant pattern by tilting angle developed in the previous study, and the two types of composite fabrics laminated with the aramid knit. Figure 3 shows a graph of bending strength and strain.

Figure 3a shows a graph of bending strength by sample, and compares by dividing the thickness by sample. First of all, the bending strength values by sample were 0.19–0.21 MPa for ARNT-n, 0.05–0.11 MPa for 3DP-RE-n, 0.09–0.18 MPa for 3DP-RE-n/ARNT-0, and 0.04–0.11 MPa for 3DP-RE-n/ARNT-n; appeared larger in the order of ARNT-n > 3DP-RE-n > 3DP-RE-n/ARNT-n > 3DP-RE-n/ARNT-0 as a result. It was also confirmed that the ARNT-n was about three times higher than the values of 3DP-RE-n/ARNT-0 and 3DP-RE-n/ARNT-n.

For the tilting angle of each sample, ARNT-n, which appeared similar to about 0.20 MPa, was found to have no difference in bending properties by tilting angle, while 3DP-RE-n and 3DP-RE-n/ARNT-n showed a tendency for increase bending strength to increase as tilting angle increases. This is confirmed that the molten filament stacking direction according to the nozzle movement direction and the aramid knit fabric influenced the bending strength of each sample tilting angle when printing a 3D printed auxetic re-entrant pattern. And for the sample with an tilting angle of 0° , the strength was found to be significant in the experiment because the direction applied to the load and the direction in which the filaments were stacked during the experiment were positioned



(a)



(b)

Fig. 3 **a** Bending strength and **b** strain at max bending strength of bending test of aramid knit, 3D printed auxetic re-entrant pattern and 3D printed auxetic re-entrant pattern/aramid knit composite with various tilting angles

perpendicular to each other, causing the most impact on the load (Somiredy & Czeksanski, 2020; Yao et al, 2020). In addition, as in the previous study, 3DP-RE-n/ARNT-n appeared similarly to the 3D printed auxetic re-entrant pattern; it was more affected by the 3D printed auxetic re-entrant pattern rather than the aramid knit fabric. On the

other hand, it was found that the bending strength of 3DP-RE-n/ARNT-0 decreases as the tilting angle increases. In the case of 3DP-RE-90/ARNT-0, the direction in which the load is applied is the same as the stacking direction of the 3D printed auxetic re-entrant pattern and the MD direction of the knit, so that the strength seems to decrease because it is less affected by the load.

Figure 3b is a graph of strain at the maximum bending strength for each sample. ARNT-n was measured to be 1.21–1.74%, 3DP-RE-n was 3.55–5.09%, 3DP-RE-n/ARNT-0 was 4.86–7.26%, and 3DP-RE-n/ARNT-n was 7.26–9.04%; appeared larger in the order of 3DP-RE-n/ARNT-n > 3DP-RE-n/ARNT-0 > 3DP-RE-n > ARNT-n as a result. When manufactured as a 3D printed auxetic re-entrant/aramid knit composite fabric, it was found to be more than four times larger than the existing aramid knit, and it was found that bending properties during the manufacture of the composite fabric.

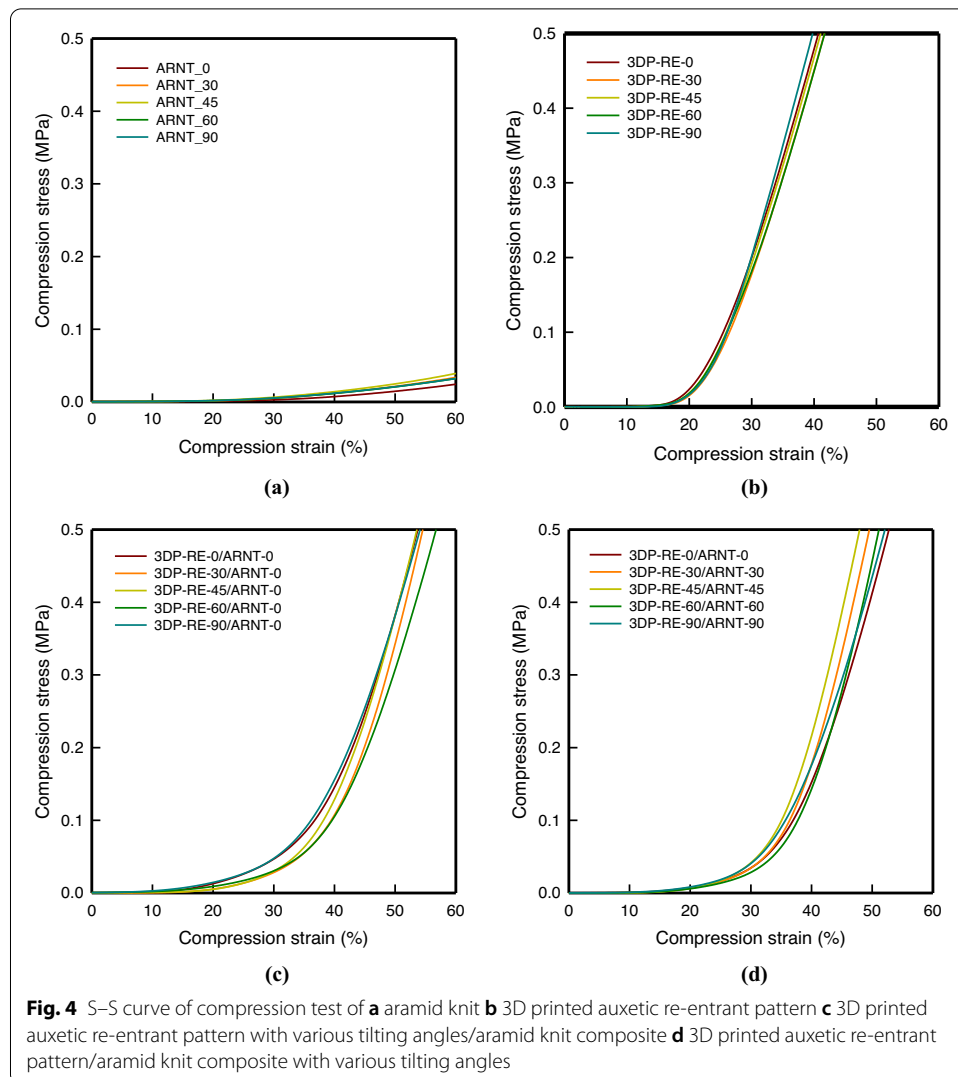
For each tilting angle, ARNT-n had the greatest strain at 45°; it is considered to be the largest because the fabric direction was the bias direction. On the other hand, 3DP-RE-n and 3DP-RE-n/ARNT-n showed the smallest strain at 45°. This composite fabric, similar to the tendency of bending strength, was found to be more affected by the 3D printed auxetic re-entrant pattern than the effect of aramid knit. On the other hand, 3DP-RE-n/ARNT-0 showed the smallest strain at 90°. In the same way as the bending strength, it is confirmed that the elongation appeared to be small because the stacking direction of the 3D printed auxetic re-entrant pattern, the MD direction of the aramid knit and the applied loading direction are the same. Therefore, when manufacturing composite fabrics, the bending strength and bending strain of 3DP-RE-n/ARNT-n, which are bonded with the same tilting angle of the aramid knit and the 3D printed auxetic re-entrant pattern, were improved.

Compression property of aramid knit, 3D printed auxetic re-entrant pattern and its two-types of composite fabrics by tilting angles

The compressive properties by tilting angle of aramid knit, 3D printed auxetic re-entrant pattern, and 2 types of 3D printed auxetic re-entrant/aramid knit composite fabric are shown in Figs. 4 and 5. Figure 4 is the compressive strength-strain curve graph, and Fig. 5 is a graph summarizing the compressive properties.

For the compressive strength-strain curve, the compression behavior appeared similar regardless of the pattern tilting angle. ARNT-n showed almost no change in compressive strength up to 50% of the compressive strain, and at 50%, compressive strength showed about 0.02 MPa, then gradually increased at 80%. However, at 100%, the compressive strain was found to be about 0.13 MPa, and it can be seen as not significantly affected by compression due to the thin fabric thickness. On the other hand, the compression strength of the 3D printed auxetic re-entrant pattern and the composite fabric increased gradually to about 20% and then rapidly increased to about 0.33 MPa after 20%, and the compressive strains at 50% were about 0.33, 0.33, and 0.40 MPa, respectively, indicating that the compressive strength was improved by more than 17 times compared to ARNT-n.

Toughness when compressed is about 1.54 J for ARNT-n, about 1.55 J for 3DP-RE-n, about 2.05 J for 3DP-RE-n/ARNT-0, and about 2.06 J for 3DP-RE-n/ARNT-n; appeared larger in the order of 3DP-RE-n/ARNT-n > 3DP-RE-n/ARNT-0 > 3DP-RE-n > ARNT-n



as a result. Accordingly, as the compressive strength and toughness were improved in the manufacture of the composite fabric, it was confirmed that the compression performance was improved because it was able to withstand the load more during compression as the 3D printed auxetic re-entrant pattern printed as the elastomer and the swelling properties that can be represented by the structural features of the aramid knit were laminated. Therefore, it is considered that the energy absorption properties of the 3D printed auxetic re-entrant pattern/aramid knit composite fabric representing excellent compressive properties will be improved than that of the substrate fabric.

Tensile property of aramid knit, 3D printed auxetic re-entrant pattern and its two-types of composite fabrics by tilting angles

This study have identified the tensile properties of the aramid knit, the 3D printed auxetic re-entrant pattern, and the 2 types of 3D printed auxetic re-entrant/aramid knit composite fabric by tilting angles. Figure 6 shows the stress–strain curve for each sample,

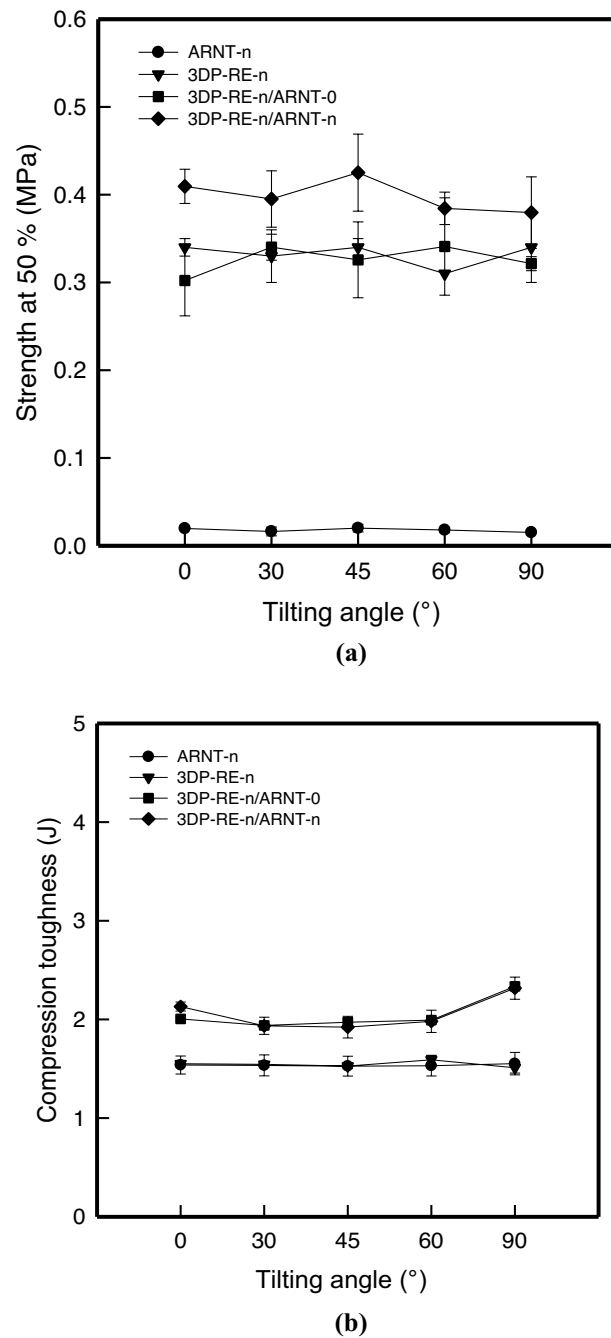
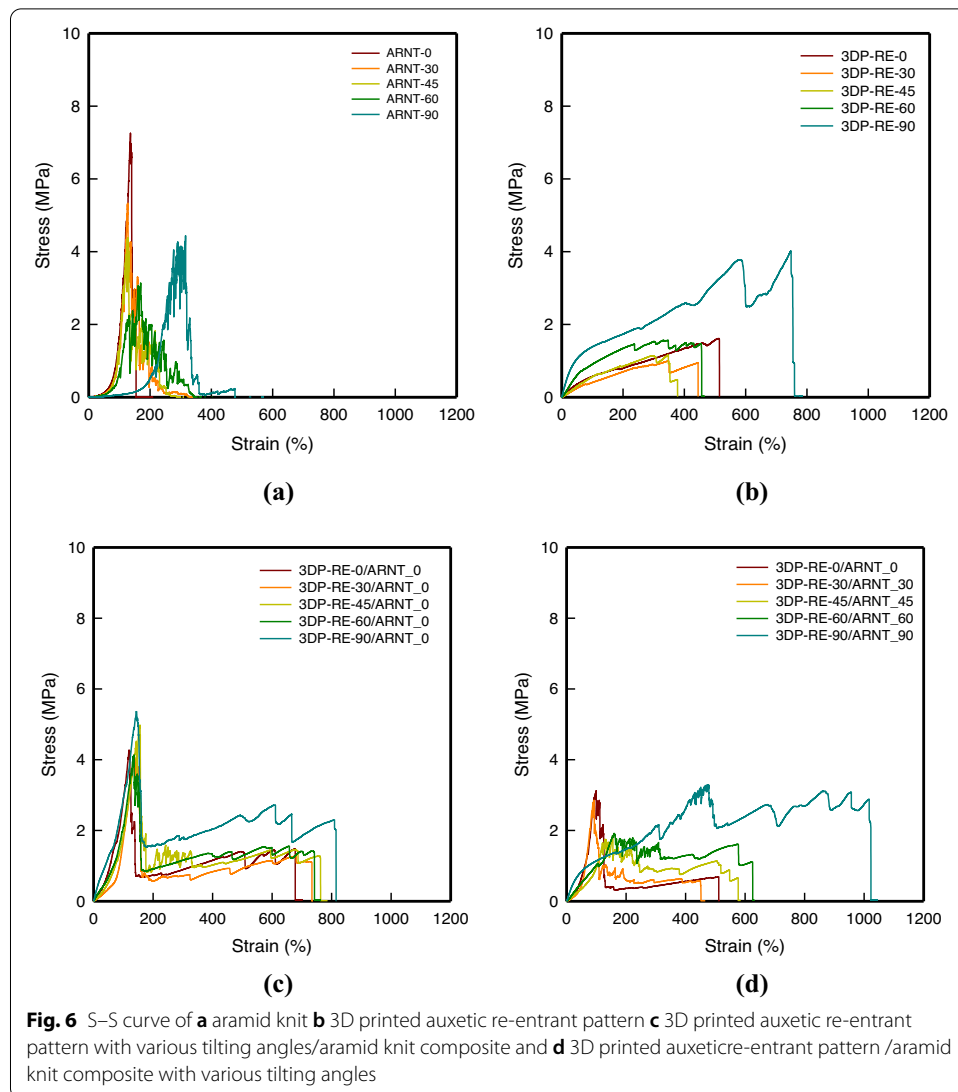


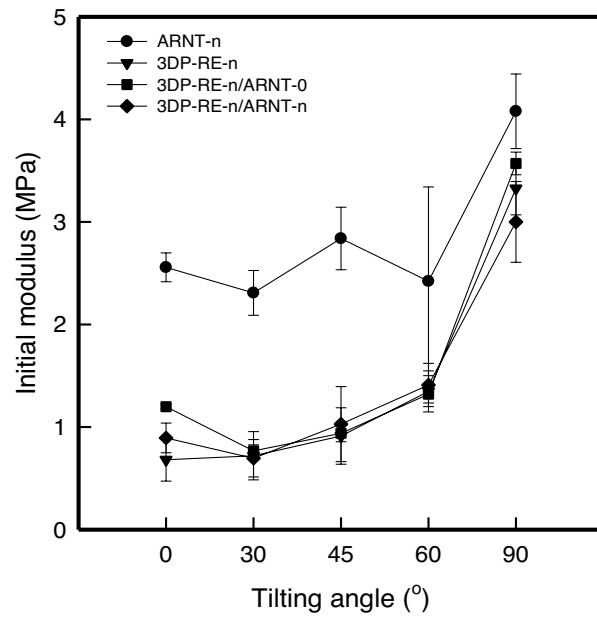
Fig. 5 Compression property of aramid knit, 3D printed auxetic re-entrant pattern and 2 types of 3D printed auxetic re-entrant pattern/aramid knit with various tilting angles

Fig. 7 shows the initial modulus and toughness, and Table 4 compares and analyzes the max stress, breaking stress, strain at max and breaking stress in the table.

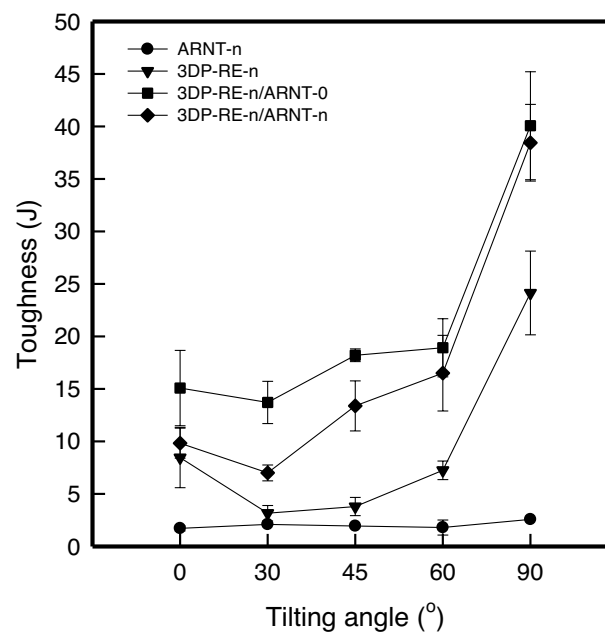
The stress–strain curve for each sample shown in Fig. 6 shows that the aramid knit was fractured at high stress and low strain in the case of ARNT-n, whereas the 3DP-RE-n was fractured at low stress and high strain. The tilting angles of the initial modulus



region of ARNT- n appeared steeper, and 3DP-RE- n was confirmed to be a more flexible material showing elastic behavior in the initial stage. 3DP-RE- n showed better tensile properties than aramid knit when printed as TPU materials with excellent elasticity. In addition, the composite fabrics 3DP-RE- n /ARNT-0 and 3DP-RE- n /ARNT- n were fractured at a high elongation similar to 3DP-RE- n , and the tilting angles of the initial modulus region was gradual. On the other hand, in the case of the tensile behavior, it can be seen that the aramid knit was first fractured, and then the 3D printed auxetic re-entrant pattern was fractured during applied loading. In addition, since 3DP-RE- n /ARNT-0 has the same tilting angles of aramid knit, it was found that until the aramid knit fracture, it had a similar tendency to ARNT-0, ARNT-30 and ARNT-45, however, after it was fractured, it was found to be affected by the 3D printed auxetic re-entrant pattern. On the other hand, 3DP-RE- n /ARNT- n show the similar tendency at 0° and 30° as ARNT-0 and ARNT-30 same as 3DP-RE- n /ARNT-0 until the aramid knit was fractured, however, 3DP-RE-45/ARNT-45, 3DP-RE-60/ARNT-60 and 3DP-RE-90/ARNT-90 were found to



(a)



(b)

Fig. 7 **a** Initial modulus and **b** tensile toughness of aramid knit, 3D printed auxetic re-entrant pattern and 2 types of 3D printed auxetic re-entrant pattern/aramid knit composite with various tilting angles

be more affected by 3D printed auxetic re-entrant pattern. It is considered that this is because the tilting angles of the aramid knit and the 3D printed auxetic re-entrant pattern increases in the same way.

Based on the S-S curve analyzed earlier, the stress and strain are shown in Table 4. First, the max stress appeared in the order of ARNT-n > 3DP-RE-n/ARNT-0 > 3DP-RE-n/

Table 4 Tensile property of aramid knit, 3D printed auxetic re-entrant pattern and 2 types of 3D printed auxetic re-entrant pattern/aramid knit composite with various tilting angles

Sample	Stress (MPa)		Strain (%)	
	Max	Breaking	At Max strain	At breaking strain
ARNT-n	6.82 ± 0.34	3.34 ± 0.37	122.10 ± 8.33	136.72 ± 6.61
	4.68 ± 1.79	0.98 ± 0.21	142.91 ± 48.84	218.03 ± 37.30
	3.93 ± 0.62	1.35 ± 0.11	124.61 ± 3.24	219.71 ± 6.69
	3.78 ± 0.93	1.35 ± 0.15	149.61 ± 43.59	251.55 ± 19.85
	4.18 ± 0.18	0.74 ± 0.14	305.05 ± 16.32	348.61 ± 15.65
3DP-RE-n	1.77 ± 0.21	1.77 ± 0.21	633.22 ± 131.56	635.21 ± 131.04
	1.02 ± 0.06	0.77 ± 0.19	358.09 ± 48.97	411.57 ± 79.20
	1.26 ± 0.15	0.57 ± 0.08	345.15 ± 9.39	393.76 ± 39.50
	1.70 ± 0.18	1.53 ± 0.09	435.90 ± 78.16	484.85 ± 27.89
	4.26 ± 0.91	3.55 ± 1.07	744.54 ± 19.98	762.17 ± 21.22
3DP-RE-n/ ARNT-0	4.17 ± 0.30	1.41 ± 0.27	121.39 ± 20.89	667.04 ± 136.71
	3.97 ± 0.44	0.81 ± 0.13	131.21 ± 5.14	765.13 ± 96.54
	4.47 ± 0.51	1.44 ± 0.14	151.85 ± 9.46	723.79 ± 30.33
	4.33 ± 0.53	1.35 ± 0.12	143.26 ± 7.86	723.79 ± 30.33
	5.02 ± 0.36	4.14 ± 0.73	154.50 ± 4.60	982.20 ± 32.63
3DP-RE-n/ ARNT-n	3.09 ± 0.05	0.55 ± 0.22	98.65 ± 0.98	721.71 ± 77.47
	2.85 ± 0.33	0.47 ± 0.10	95.44 ± 2.50	455.66 ± 72.23
	2.00 ± 0.13	0.49 ± 0.02	138.47 ± 15.64	640.99 ± 57.37
	2.09 ± 0.15	0.52 ± 0.10	230.24 ± 75.44	641.40 ± 74.72
	3.10 ± 0.24	1.79 ± 0.14	454.98 ± 19.48	943.71 ± 08.09

ARNT-n > 3DP-RE-n, and the aramid knit was found to be the strongest material as a result. In addition, as confirmed in the stress–strain curve, the max stress of 3DP-RE-n/ARNT-0 is considered to be large under the influence of aramid knit, and 3DP-RE-n/ARNT-n is considered small under the influence of the 3D printed auxetic re-entrant pattern. In the case of ARNT, as the thread fell out after the fabric was partially fractured, the breaking stress appeared to be more than 50% smaller than the max stress, and 3DP-RE-n appeared similar to the max stress, after the specimen was completely fractured at the end during tensioning under the influence of TPU. In the case of 3DP-RE-n/ARNT-0 and 3DP-RE-n/ARNT-n, only the 3D printing auxetic re-entrant pattern was fractured during tensioning after the aramid knit was broken first, and the fracture strength was found to be 33% less than the max stress at the tilting angles excluding the tilt of 90°.

Next, the strain at the max stress was small in the order of 3DP-RE-n > ARNT-n > 3DP-RE-n/ARNT-n > 3DP-RE-n/ARNT-0. And the strain at breaking stress was small in the order of 3DP-RE-n/ARNT-0 > 3DP-RE-n/ARNT-n > 3DP-RE-n > ARNT-n. ARNT-n and 3DP-RE-n were similar to the strain at max and breaking stress with the same tendency as the stress. The elongation at the max stress and the strain at breaking stress of the composite fabrics 3DP-RE-n/ARNT-0 and 3DP-RE-n/ARNT-n were found to be affected by the aramid knit fabric that was fractured first, after then it was shown that affected by the 3D printed auxetic re-entrant pattern.

When comparing stress and strain by tilting angle, the strength of ARNT-0 and ARNT-90 at ARNT-n was first measured greater than ARNT-30, ARNT-45 and ARNT-60.

3DP-RE-n, 3DP-RE-n/ARNT-0, and 3DP-RE-n/ARNT-n were all measured highest at 90°. This tends to be the same as in the previous study (Kim et al., 2020) because the stacking and tensile directions of the 3D printed auxetic re-entrant pattern are greatly affected by the load in the opposite direction. Next, the strain of ARNT-n was measured the highest at ARNT-90. 3DP-RE-n increased in the order of 3DP-RE-45 < 3DP-RE-30 < 3DP-RE-60 < 3DP-RE-0 < 3DP-RE-90. It was confirmed that the samples in the tilting angles of 0° and 90° with the same tendency as the stress have the superior stress and strain that the samples in the bias direction. The stress and strain of the composite fabrics 3DP-RE-n/ARNT-0 and 3DP-RE-n/ARNT-n were also confirmed to be excellent in the direction of tilting angles of 0° and 90°.

As the initial modulus can be seen in the stress–strain curve of Fig. 7a, 3DP-RE-n, 3DP-RE-n/ARNT-0, 3DP-RE-n/ARNT-n have been found to be more flexible than ARNT-n due to the influence of the 3D printed auxetic re-entrant pattern, and the initial modulus tended to increase as the tilting angle increased. All samples also showed the best at an tilting angle of 90°. The toughness shown in Fig. 7b was greater in the order of 3DP-RE-n/ARNT-0 > 3DP-RE-n/ARNT-n > 3DP-RE-n > ARNT-n. The toughness by tilting angle of ARNT-n showed no significant difference. On the other hand, 3DP-RE-n, 3DP-RE-n/ARNT-0, and 3DP-RE-n/ARNT-n were the best at an tilting angle of 90°. Therefore, when manufactured as a composite fabric, the durability of these fabrics was confirmed to have been improved because their toughness was increased as compared with the existing aramid knit and the 3D printed auxetic re-entrant pattern.

Conclusion

This study was attempted to confirm the applicability of aramid knit, 3D printed auxetic re-entrant pattern, and two types of aramid knit laminated with 3D printed auxetic re-entrant pattern to the shoe uppers in consideration of the analysis on the Poisson's ratio bending properties, compressive properties and tensile properties by tilting angles.

In the results of the Poisson's ratio of 3DP-RE-n and 3DP-RE-n/ARNT-0 showed negative values at all tilting angles and identified as auxetic structures. In the case of increasing tilting angles of 3DP-RE-n/ARNT-n showed a negative, whereas a positive Poisson's ratio of more than 25.5% at 0° and 90°. Almost samples showed the largest shear deformation of the 3D printed auxetic re-entrant pattern at 60°. In the results of the bending property, there is no significant difference in bending strength by tilting angles of ARNT-n, and the bending strength of 3DP-RE-n and 3DP-RE-n/ARNT-n increased as tilting angles increased. The strain at the max bending strength was low in the bias direction. For 3DP-RE-n/ARNT-0, the MD direction of the aramid knit and the stacking direction of the 3D printed auxetic re-entrant pattern coincided with the direction in which the load is applied, resulting in a decrease in bending strength and strain. The compressive properties did not differ significantly in strength and toughness by tilting angles, and the strength and toughness with a strain of 50% were found to be improved in the manufacture of the composite fabric in the order of 3DP-RE-n/ARNT-n > 3DP-RE-n/ARNT-0 > 3DP-RE-n > ARNT-n. As a result of the tensile properties, the initial modulus, strain, and toughness of 3DP-RE-n, 3DP-RE-n/ARNT-0 and 3DP-RE-n/ARNT-n were greater, and were found to be the greatest especially at a tilting angle of 90°. The max stress of 3DP-RE-n/ARNT-n laminated with the 3D printing auxetic re-entrant pattern

and 3DP-RE-n/ARNT-n at the same tilting angle showed a great max stress at the tilting angle of 0° and 30° due to the influence of the aramid knit. However, it was found to be more affected by the 3D printed auxetic re-entrant pattern at the tilting angle of 45°, 60° and 90°.

In this study, it has been confirmed that the mechanical properties of the composite fabric in which aramid knit and 3D printed auxetic re-entrant pattern were laminated have improved. It is considered that a composite fabric with improved mechanical properties including flexibility and toughness, and morphological stability by adding a 3D printed auxetic re-entrant structure to the aramid knit with the excellent properties such as high strength and heat resistance properties can be applied to the shoe uppers of high-functional safety and protection shoes.

Acknowledgements

Not applicable.

Authors' information

Imjoo Jung is a Graduate student at the Dong-A University. Heylim Kim is a researcher at the Research Institute of Convergence Design in Dong-A University. Sunhee Lee is a professor at the Dong-A University.

Authors' contributions

SL conceived the work and IJ & HK prepared the samples and performed the experiments. IJ, HK and SL are participated in the sequence alignment and drafted the manuscript. All authors read and approved the final manuscript.

Funding

This work was supported by the National Research Foundation of Korea (NRF) granted funded by the Korea government (MSIP) (No. NRF-2019R1A2C2084041).

Availability of data and materials

The data sets used and analyzed during the current study are available from the corresponding author on reasonable request.

Declarations

Competing interests

The authors declare that they have no competing interests.

Author details

¹Graduate Student, Department of Fashion and Textiles, Dong-A University, Busan 49315, Republic of Korea. ²Researcher, Research Institute of Convergence Design, Dong-A University, Busan 49315, Republic of Korea. ³Professor, Department of Fashion Design, Dong-A University, 37 Nakdong-Daero, Saha-gu, Busan 49315, Republic of Korea.

Received: 10 March 2021 Accepted: 30 June 2021

Published online: 25 December 2021

References

- Abtew, M. A., Boussu, F., Bruniaux, P., Loghin, C., & Cristian, I. (2019). Engineering of 3D warp interlock p-aramid fabric structure and its energy absorption capabilities against ballistic impact for body armour applications. *Composite Structures*, 225, Article 111179. <https://doi.org/10.1016/j.compstruct.2019.111179>
- Grimmelsmann, N., Meissner, H., & Ehrmann, A. (2016). 3D printed auxetic forms on knitted fabrics for adjustable permeability and mechanical properties. *IOP Conference Series: Materials Science and Engineering* 137, Article 012011. <https://doi.org/10.1088/1757-899X/137/1/012011>
- Han, I. S., Kim, D. S., Lee, J. Y., Kim, O. H., & Park, T. H. (2011). Usage development trend of Para-aramid fiber. *Fiber Technology and Industry*, 15(1), 7–15.
- Han, I. S., & Lee, C. B. (2006). Characteristics and application of aramid fiber. *Fiber Technology and Industry*, 10(4), 339–349.
- Jung, J. Y., Ku, P., Kim, D. H., Kwon, M. J., Kang, S., Choi, J. Y., & Lee, J. Y. (2019). Development of firefighters' personal protective clothing with nomex honeycomb fabric and its protective and comfort evaluation. *Fashion & Textile Research Journal*, 21(5), 606–617. <https://doi.org/10.5805/SFTI.2019.21.5.606>
- Kabir, S., Kim, H. L., & Lee, S. H. (2020a). Characterization of 3D printed auxetic sinusoidal patterns/nylon composite fabrics. *Fibers and Polymers*, 21, 1372–1381. <https://doi.org/10.1007/s12221-020-9507-6>
- Kabir, S., Kim, H. L., & Lee, S. H. (2020b). Physical property of 3D-printed sinusoidal pattern using shape memory TPU filament. *Textile Research Journal*, 90(21–22), 2399–2410. <https://doi.org/10.1177/0040517520919750>
- Kamrul, H., Zulifqur, A., & Hu, H. (2020). Deformation behavior of auxetic woven fabric based on re-entrant hexagonal geometry in different tensile directions. *Textile Research Journal*, 90(3–4), 410–421. <https://doi.org/10.1177/0040517519869391>

- Kim, H., Kabir, S., & Lee, S. (2021). Mechanical properties of 3D printed re-entrant pattern/neoprene composite textile by pattern tilting angle of pattern. *Journal of the Korean Society of Clothing and Textile*, 45(1), 106–122. <https://doi.org/10.5850/JKSC.2021.45.1.106>
- Kim, H. L., & Lee, S. H. (2020). Mechanical properties of 3D printed re-entrant pattern with various hardness types of TPU filament manufactured through FDM 3D printing. *Textile Science and Engineering*, 57(3), 166–176. <https://doi.org/10.12772/TSE.2020.57.166>
- Kolken, H. M. A., & Zadpoor, A. A. (2017). Auxetic mechanical metamaterials. *The Royal Society of Chemistry*, 7, 5111–5129. <https://doi.org/10.1039/C6RA27333E>
- Korean Agency for Technology and Standards. (2017a). KS M ISO 527 Plastics-Determination of tensile properties. <https://e-ks.kr/streamdocs/view/sd;streamdocId=72059199179197815>. Accessed 26 Feb 2021
- Korean Agency for Technology and Standards. (2017b). KS M ISO 14125 Fiber-reinforced plastic composites-Determination of flexural properties. <https://e-ks.kr/streamdocs/view/sd;streamdocId=72059203756722767>. Accessed 26 Feb 2021
- Lakes, R. S. (2017). Negative-poisson's-ratio materials_auxetic solids. *Annual Review of Materials Research*, 47, 63–81. <https://doi.org/10.1146/annurev-matsci-070616-124118>
- Lee, S. H. (2018). Evaluation of mechanical properties and washability of 3D printed lace/voil composite fabrics manufactured by FDM 3D printing technology. *Fashion & Textile Research Journal*, 20(3), 353–359. <https://doi.org/10.5805/SFTI.2018.20.3.353>
- Li, T., Chen, Y., Hu, X., Li, Y., & Wang, L. (2018). Exploiting negative Poisson's ratio to design 3D-printed composites with enhanced mechanical properties. *Materials and Design*, 142, 247–258. <https://doi.org/10.1016/j.matdes.2018.01.034>
- Li, T., & Wang, L. (2017). Bending behavior of sandwich composite structures with tunable 3D-printed core materials. *Composite Structures*, 175, 46–57. <https://doi.org/10.1016/j.compstruct.2017.05.001>
- Novak, N., Dubrovski, P. D., Borovinsek, M., Vesenjaj, M., & Ren, Z. (2020). Deformation behaviour of advanced textile composites with auxetic structure. *Composite Structures*, 252, Article 112761. <https://doi.org/10.1016/j.compstruct.2020.112761>
- Roy, R., Laha, A., Awasthi, N., Majumdar, A., & Butola, B. S. (2018). Multi layered natural rubber coated woven P-aramid and UHMWPE fabric composites for soft body armor application. *Polymer Composites*, 39(10), 3636–3644. <https://doi.org/10.1002/pc.24391>
- Somireddy, M., & Czekaniki, A. (2020). Anisotropic material behavior of 3D printed composite structures—Material extrusion additive manufacturing. *Materials and Design*, 195, Article 108953, 1–12. <https://doi.org/10.1016/j.matdes.2020.108953>
- Wang, X., Zhang, J., Bao, L., Yang, W., Zhou, F., & Liu, W. (2020). Enhancement of the ballistic performance of aramid fabric with polyurethane and shear thickening fluid. *Materials and Design*, 196, Article 109015. <https://doi.org/10.1016/j.matdes.2020.109015>
- Yang, C., Vora, H. D., & Chang, Y. (2018). Behavior of auxetic structures under compression and impact forces. *Smart Material and Structures*, 27(2), Article 025012 <https://doi.org/10.1088/1361-665X/aaa3cf>
- Yao, T., Ye, J., Deng, Z., Zhang, K., Ma, Y., & Ouyang, H. (2020). Tensile failure strength and separation angle of FDM 3D printing PLA material: Experimental and theoretical analyses. *Composites, Part B: Engineering*, 188, Article 107894. <https://doi.org/10.1016/j.compositesb.2020.107894>
- Zhao, S., Hu, H., Kamrul, H., Chang, Y., & Zhang, M. (2020). Development of auxetic warp knitted fabrics based on reentrant geometry. *Textile Research Journal*, 90(3–4), 344–356. <https://doi.org/10.1177/0040517519866931>

Publisher's Note

Springer Nature remains neutral with regard to jurisdictional claims in published maps and institutional affiliations.

Submit your manuscript to a SpringerOpen[®] journal and benefit from:

- Convenient online submission
- Rigorous peer review
- Open access: articles freely available online
- High visibility within the field
- Retaining the copyright to your article

Submit your next manuscript at ► [springeropen.com](https://www.springeropen.com)